Renewable Energy 88 (2016) 30–39

Contents lists available at ScienceDirect

Renewable Energy

journal homepage: www.elsevier.com/locate/renene

Kinetic energy extraction of a tidal stream turbine and its sensitivity to structural stiffness attenuation

C.E. Morris [c], D.M. O'Doherty [b], T. O'Doherty [a], A. Mason-Jones [a, *]

[a] Mechanical, Manufacturing and Medical Engineering, School of Engineering Cardiff University, UK
[b] School of Engineering, Facility of Computing, Engineering and Science, University of South Wales, UK
[c] Engineering Design and Mathematics, Faculty of Environment and Technology, University of The West of England, UK

ARTICLE INFO

Article history:
Received 18 August 2014
Received in revised form
18 August 2015
Accepted 19 October 2015
Available online 19 November 2015

Keywords:
CFD
FEA
Tidal stream turbine
FSI
TST

ABSTRACT

The hydrodynamic forces imparted on a tidal turbine rotor, whilst causing it to rotate and hence generate power, will also cause the blades to deform. This deformation will affect the turbine's performance if not included in the early design phase and could lead to a decrease in power output and a reduction in operational life. Conversely, designing blades to allow them to deform slightly may reduce localised stress and therefore prolong the life of the blades and allow the blades to deform in to their optimum operational state. The aim of this paper is to better understand the kinetic energy extraction by varying the material modulus of a turbine blade. Shaft torque/power, blade tip displacement, and axial thrust results are presented for 2, 3 and 4 bladed rotor configurations at peak power extraction. For the rotor design studied the FSI model data show that there is a low sensitivity to blade deformation for the 2, 3 and 4 bladed rotors. However, the results reveal that the 3 bladed rotor displayed maximum hydrodynamic performance as a rigid structure which then decreased as the blade deformed. The 2 and 4 bladed rotor configurations elucidated a slight increase in hydrodynamic performance with deflection.

© 2015 The Authors. Published by Elsevier Ltd. This is an open access article under the CC BY license (http://creativecommons.org/licenses/by/4.0/).

1. Introduction

The EU has targeted renewable Energy to provide 20% of the total energy mix by 2020 [1] in comparison the UK target is 15% of the UK energy demands from renewable sources by 2020 [2]. From statistics published by the Department of Energy and Climate Change (DECC) since 2008, wind energy has been the largest contributing renewable source to the energy mix. In 2012 a total of 8.8% of the UKs electricity demand came from renewable resources, more than half (5.48%) of which came from the wind sector [3]. The annual growth of the wind energy sector is significant, yet remains dependent on unpredictable wind conditions and hence a steady base load. In order to meet and sustain the targets set by 2020 and beyond, the UK and EU at large must continue to address the imbalance in the renewable energy mix.

To add to this renewable mix the potential for sustainable production through wave and tidal energy conversion has resulted in large investment from industry and governments. For example, the Carbon Trusts Marine Energy Accelerator program has identified a practical and economical resource of tidal current and wave energy resource of 70 TWh/yr around the UK coast, which would contribute to 20% of UK's total industrial, commerce and domestic electricity demands based on 2012 usage [4].

The long term predictability of tides is the main advantage of tidal power over wind and solar, since it allows any phase change in power productions between wind and or other tidal stream and wave sites to be balanced. The two leading techniques in energy conversion for tidal range power generation are impoundment schemes such as a barrage or tidal lagoon. These techniques yield reward for large scale solutions, as documented in the La Rance Tidal Power Plant run by EDF Energy which produces 0.54 TWh/year. In the short term damage to the local ecosystem occurred however this was mainly during the construction stages [5]. Large capital investments and resulting ecological damage and aesthetic disturbance creates acceptance of such schemes difficult, although the tidal lagoon based in Swansea Bay, South Wales, UK has submitted an application for development which is still awaiting consent [6]. An alternative to tidal range power generation is via

* Corresponding author. School of Engineering, Cardiff University, Queen's Buildings, The Parade, Cardiff, UK.
E-mail addresses: ceri.morris@uwe.ac.uk (C.E. Morris), daphne.odoherty@southwales.ac.uk (D.M. O'Doherty), odoherty@cardiff.ac.uk (T. O'Doherty), mason-jonesa@cardiff.ac.uk, mason-jonesa@cf.ac.uk (A. Mason-Jones).

http://dx.doi.org/10.1016/j.renene.2015.10.037
0960-1481/© 2015 The Authors. Published by Elsevier Ltd. This is an open access article under the CC BY license (http://creativecommons.org/licenses/by/4.0/).

the use of a Tidal Stream Turbines (TSTs). These devices are optimised for their location, to maximise kinetic energy extraction from free flowing water. Being submerged a TST is by its nature significantly less intrusive than impoundment schemes and minimises impacts on the marine and costal environment. In spite of some TST designs involving support structures that penetrate the water's surface this technique is still considerably less aesthetically intrusive than other large scale renewable energy technologies.

The introduction of TSTs into the UK energy mix can only be a positive step since the UK has some of the strongest currents in the world. Areas around Orkney Islands, Pentland Firth, Anglesey and Pembrokeshire, have been studied as viable sites for installing tidal energy devices [7]. Ideal conditions for tidal stream turbines are; a free stream velocity of 2–3 m/s and a depth of 20–30 m, at least for early stage implementation with deeper water designs (>40 m) introduced as the industry matures. Tidal Energy Limited is currently developing their DeltaStream device for 12 month test in the Ramsey Sound, Pembrokeshire. Marine Current Turbines (MCT) developed and installed the first commercially operating tidal stream turbine. The SeaGen S is a 1.2 MW capacity gull-wing horizontal axis TST installed in Strangford Lough, Northern Ireland since 2008. The 16 m diameter twin rotors positioned at either end of the supporting gull wing are pitch controlled. From environmental monitoring reports actively pitch controlling the blades limits the maximum rotational speed of the rotors to 14RPM [8]. The hydrodynamic forces required to produce such motion will also cause considerable loading on the blades which will result in blade deformation. The magnitude of the deformation will be dependent on the external and internal structure of the blades and the materials used.

2. Performance of 2, 3 and 4 bladed rotor

The aim of this work was to investigate, by the means of coupled 2 way FSI modelling, the extent of blade deformation and the associated changes in hydrodynamic performance characteristics. Note is made of the kinetic energy extraction sensitivity by varying the material modulus and hence the stiffness of the rotor structure. Although not discussed in this paper the axial loading and shaft torque data generated will be used as part of the development of a conditioned based monitoring system [9]. The data generated in this study and a further 2-way transient model will be subsequently validated using a lab scale rotor.

Generally when using Computational Fluid Dynamics (CFD) the hydrodynamics of a turbine blade are studied while in its undeformed state and therefore is considered as being rigid. While this approach might serve well at the prototype phase, it is unlikely to suit the operation of a large scale device. Blade deflection will depend on the internal structure, the materials used and the profile shape, for example long slender blades. Using a 3D coupled boundary element method and finite element method Yin [10] showed that when scaled to 20 m a rotor with long slender blades led to excessive blade bending and high localised stresses when run outside its optimal operational conditions. Therefore, when scaling a device to economically viable dimensions, numerical modelling can play an important role in informing engineers on the magnitudes of deflections and potential for stress raisers. . There are however a number of issues facing the development of turbine blades via numerical simulation, such as the number of development iterations and the time it takes to run the numerical simulations when using fully coupled 2 way FSI simulations. Numerical run-time, to some extent, is a product of processing speed and the accuracy required to capture the physics of the real system, the latter being dependent on the numerical approach.

There are a number of theories that can be used to model the hydrodynamic performance of TSTs with a good degree of accuracy. The most prominent of these is the Blade Element Momentum Theory (BEMT) which is a combination of the momentum and blade element theories, [11]. Resulting from their work on experimental verification of numerical predictions using a 0.8 m diameter rotor, Bahaj [12] and Batten [13] demonstrated that power and thrust measurements showed good correlation with those obtained using the BEMT. Barltrop [14] also used the BEMT to investigate the effects of waves on marine current turbines and their influence on blade root bending moments. Other approaches include the Vortex method which has the ability to include 3D flows. Malki et al. [15] have developed a coupled BEM–CFD model which is based on momentum source terms from a BEM model being fed into a RANS model. The authors state that where the incoming flow is non-uniform, as is likely in most practical cases, this method can give more realistic predictions than the classical BEM method.

Batten et al. [16] have also used this method and state that it is suitable for assessing the interactions of wakes in an array but not for obtaining predictions for the loading on each individual blade since the time-averaged nature of the actuator disk still applies. In combination with the Finite Element Method (FEM) an FSI study can be used to predict the deformation of the blade and its resulting influence on the hydrodynamics of the blade. The main advantage of the above methods is that they are computationally inexpensive with good accuracy. However, as the near field flow regime is influenced by say the wake of an upstream turbine, local bathymetry and support structure, such as a stanchion, a more refined solution is required. As the complexity of the flow increases CFD methods are better suited to capture the near field hydrodynamics of the system. Challenging flows such as these are further complicated by the directionality of the tide and its influence on Fluid Structure Interaction (FSI). Previous FSI studies of marine turbines include Nicholls-Lee [17] where a loosely coupled approach was applied to the FSI modelling via a surface panel code for the CFD and ANSYS 12.1 for the Finte Element Analsys (FEA). Matlab was used as the FS interface to enable the transfer of force and displacement data between the CFD and FEA codes. This work gives a valid insight to the effects of fluid structure interaction and its consequences on cavitation, power attenuation and stresses on the structure. While it is stated by Ref. [17] that the panel method performs well for undeviating flows it was also highlighted that at a more advanced development stage, such as where it becomes necessary to include intricacy in the hydrodynamic flow field, the Reynolds Averaged Navier–Stokes (RANS), Detached Eddy Simulation (DES) and Large Eddy Simulation (LES) solvers will be required for the CFD to accurately capture the hydrodynamics. Moreover, with an increased knowledge of a hydrodynamic flow field under extreme conditions such as: an upstream velocity profile and fluid structural interaction it becomes necessary to consider the possibility of a strong coupling effect between the fluid and a support structure. A fully coupled 2-way FSI study using a symmetry boundary and single blade was undertaken by Park et al. [18] using ANSYS CFX 13.0 and ANSYS Transient Structural. It was suggested by Ref. [18] that although the deflection of the blade was relatively small, it was still necessary to consider blade deformation due to a 1.7% drop in maximum power extraction and therefore its implication on long term rotor performance. Moreover, the latter research indicated that a possible over estimate of the maximum negative pressure on the suction side of the blade has the potential to lead to a corresponding over prediction for the initiation of cavitation. This study includes rotors with three different blade configurations to study the effect of the number of blades on deflection and hence power attenuation.

3. Fluid structure interaction (FSI) model

To establish the performance characteristics of a TST, while allowing for blade deformation, a series of coupled 2-way FSI models were constructed with a plug flow inlet boundary condition. Kinetic energy extraction and its sensitivity to structural stiffness attenuation was investigated by incrementally reducing material modulus and noting its effect on the rotor's performance. This procedure was repeated for a 2, 3 and 4 blade rotor [19].

The turbines modelled utilised a Wortmann FX 63-137 profile, with a 33° twist from the blade root to tip. The blade tip pitch angle was set to 3°, 6° and 9° with tip speed ratios (λ) of 4.4, 3.6, and 3.4 for the 2, 3 and 4 bladed rotors respectively. The λ represent peak power extraction of the rotor blades in an undeformed state [20]. The CFD models used to calculate the optimum pitch angle and λ were validated using a recirculating water flume, located at the University of Liverpool [21], and [22]. The FSI models however were not validated, but since this study does not consider the stress and strain of the blades and we are only intersted in how deflection effects the power attenuation, the mechanical analysis was only used as a tool to drive deflection and study its effect on the hydrodynamic performance.

3.1. Computational fluid dynamics model

Ansys Fluent was used to model the flow field around the turbine, Ansys Fluent uses the cell centred finite volume method with an implicit solver [24]. To ensure the turbine was isolated from any boundary effects associated with the water surface and side walls, a CFD domain entitled 'channel' was defined as having a square cross-section of 50 m by 50 m (5D × 5D turbine diameters) and a downstream length of 40D [23]. The effect of the water surface was not included due to computational restrictions associated with the additional cells that would be required. The cells within the channel were modelled in a non-accelerating coordinate system separated by a non-conformal interface between its self and the turbine volume. To simulate rotor rotation a Moving Reference Frame (MRF) was used where a rotating component is added to the fluid about the rotational axis of the turbine. Fig. 1 shows the CFD mesh within the region of the MRF [A] and rectangular channel mesh surrounding the MRF [B]. The cell density was equivilant to [21] which was shown to be grid independent. The turbine volume was centred within the channel domain cross-section, and located 10D downstream from the inlet boundary. To represent the seabed mounting height the rotational axis of the turbine was located 15 m above the seabed boundary wall. No local bathymetry features or

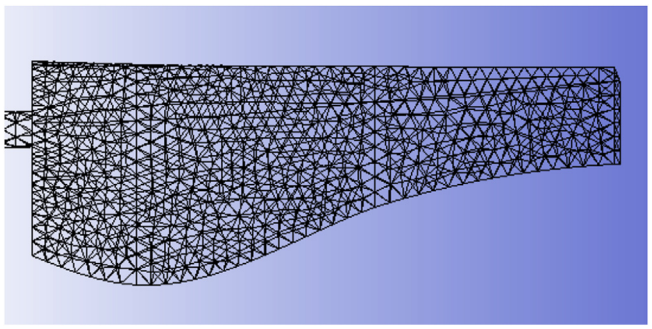

Fig. 2. Structural mesh for FSI model.

obstructions where applied to the seabed throughout the channel domain. Zero shear was applied to the side walls and surface boundaries and no-slip to the seabed boundary wall.

To limit poor numerical diffusion near the MRF non-conformal interface [D] and the tips of each blade without adversely affecting the numerical expense, a clearance of ~40% of blade length was used based on results obtained from a mesh independency study [21]. The scheme used to mesh the turbine utilised face sizing with a large density of cells at the blade tips [C], and a reducing cell density toward the hub, as also shown in Fig. 1. It should be noted that in practise under steady state conditions there is no relative motion between the nodes attached to the non-conformal interfaces. The CFD models were developed in this manner to allow for future transient modelling. As an addition the procedure also allows future transient simulations to be run using the same models. The k-ω Shear Stress Transport 2 equation turbulence model was used to close the RANS equations. The dynamic meshing option was enabled within Fluent to allow mesh deformation resulting from blade deflection in the structural model. The updated fluid mesh was controlled using both smoothing and remeshing to help prevent negative cell volumes during system coupling. Depending on model convergence either the Spring or the Diffusion smoothing method was used. With the spring smoothing method the displacement of each node is opposed by a force which is proportional to the distance. The damping of the springs is controlled by the spring constant factor which is between 0 and 1 with 0 being no damping. This was set to 1. Diffusion smoothing offers more control over which areas of the mesh are allowed to deform. Areas with low diffusivity are allowed to deform more. A diffusion parameter is specified which determines the diffusivity of a cell based on either its distance from the moving boundary or its

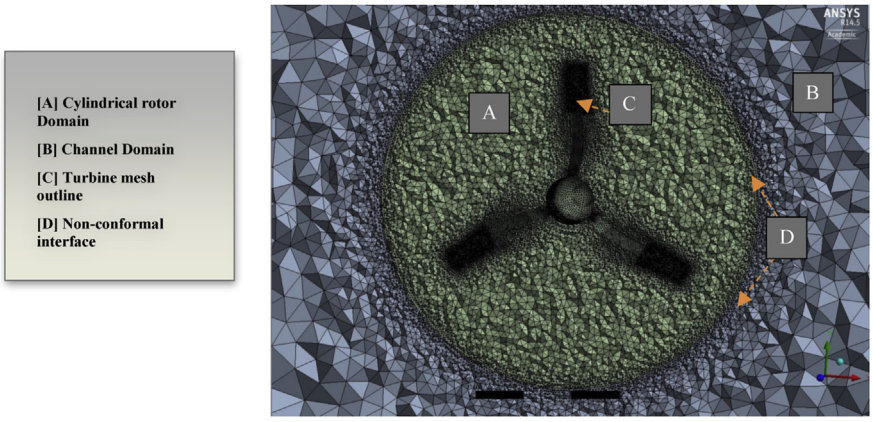

Fig. 1. Rotor mesh density within MRF and along blade surface.

volume. This means that a higher mesh quality can be preserved near the moving boundary or in areas of high cell density and therefore generally results in a better mesh than when the spring smoothing method is used, but at a higher computational cost [24]. Where the Diffusion method was used the boundary-distance option was selected for the diffusion function with a diffusion parameter of 1.5. Where remeshing was applied default parameters were selected with the minimum and maximum length scales taken from the mesh scale information panel.

3.2. Structural FEA model

The rotor structure was modelled using ANSYS Mechanical within WorkBench 14.5. In order to determine the deformation of the turbine the CFD model was coupled to the static-structural model using system coupling. The hydrodynamic forces calculated in the CFD model were transferred via system coupling to the element surfaces in the structural model. The turbine blades were meshed with a uniform element density for the structural model using 3D solid felements where each of the turbine blades was assigned a Fluid–Solid interface number. Centrifugal forces were introduced to the structural analysis via an angular velocity about the rotational axis of the rotor. To include centrifugal forces the angular velocity was set to match that of the MRF in the CFD model. The incremental time step was set to give the same number of solver iterations per coupling step as the fluid model. The rear surface of the hub was used as the support for the structure, preventing translational and rotational movement of the rear hub surface in the primary axis via a remote displacement constraint. Fixed time stepping was used and the large deflection option was selected which utilises the Newton–Raphson method. To enable a 2-way coupling analysis the 'System Coupling' procedure was used within ANSYS, where the mechanical model was first in the coupling sequence [24]. This process solves the CFD model and provides the hydrodynamic forces exerted on the blades via the fluid–solid interfaces. Following convergence of the CFD model the structural model is started within the system coupling and the hydrodynamic forces are transferred to the structural model which in turn iterates the solution to convergence. Given the specified material properties this allows the displacement of the blades to be calculated. The displacement results are then fed back to the CFD model so that the fluid mesh is deformed to match. This process is then re-iterated via the system coupling. To model any change in performance as a result of increasing blade deflection, the material modulus was reduced. Since this paper is primarily concerned with changes in hydrodynamic performance with blade deflection and not with the structural integrity of the blades no stress or strain data will be discussed but will be the topic of further work. As a

Table 1
Mapping summary.

Data transfer		
Diagnostic	Source side (%)	Target side (%)
Data transfer 1		
Percent nodes mapped	95	99
Percent area mapped	93	95
Data transfer 2		
Percent nodes mapped	95	99
Percent area mapped	93	95
Data transfer 3		
Percent nodes mapped	95	99
Percent area mapped	93	95
Data transfer 4		
Percent nodes mapped	N/A	99
Data transfer 5		
Percent nodes mapped	N/A	99
Data transfer 6		
Percent nodes mapped	N/A	99

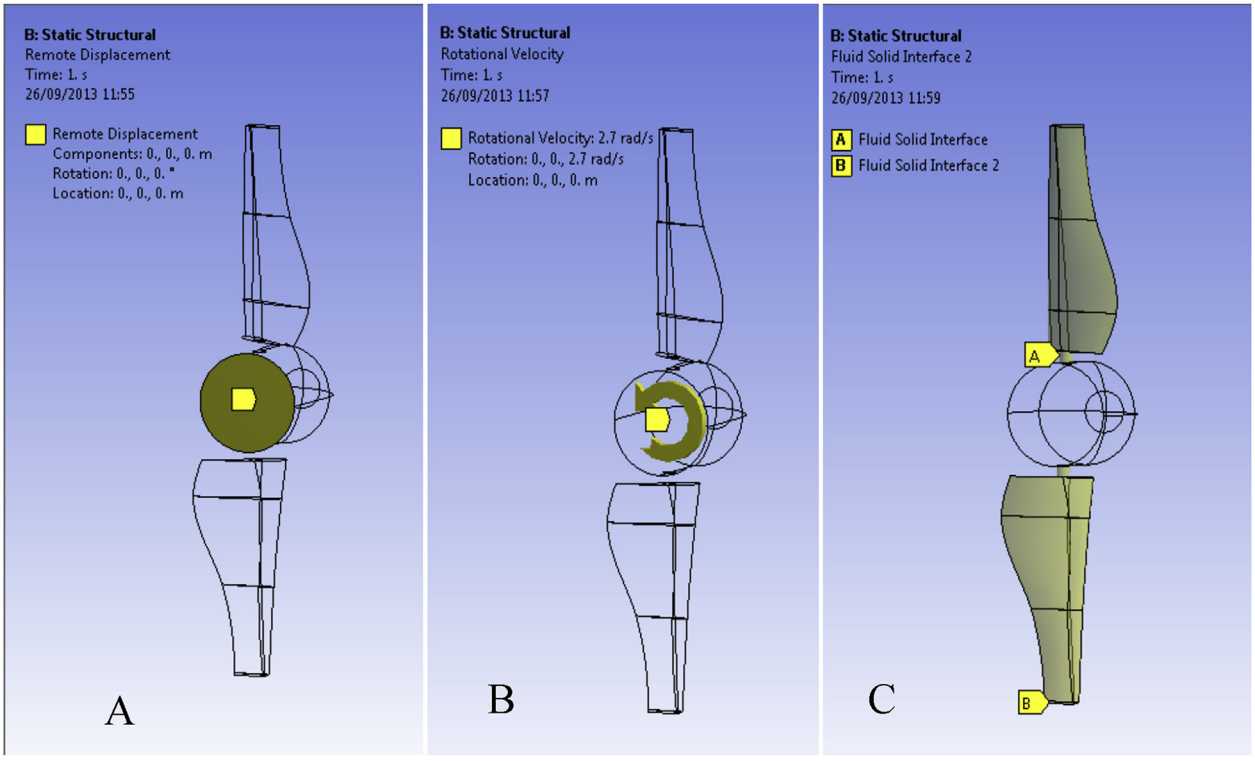

Fig. 3. Constraints and loads on FEA model.

point to note, the upstream inlet velocity in all the CFD models was a plug flow set to 3.086 m/s. A near wall velocity profile was allowed to develop at the 'seabed' using no-slip boundary condition.

The mesh for the FEA models was controlled by the use of face sizing. Since the mapping was dependent on having cells of a similar size on the coupled faces, the mesh on the surface of each blade was assigned a face size of 0.09 m, Fig. 2.

3.3. Materials

Although it is unlikely that the blades of full size turbines will be constructed with a solid internal structure, it was not necessary to develop a detailed blade structure as the study was only aimed at the hydrodynamic effects as the blade deforms with decreasing material stiffness. Hence, for simplicity the blades were modelled as solid bodies in the FEA model. This approach also helped reduce computational expense in the fully coupled scheme. It is also recognised that in reality the mass of the blades used in this study would be prohibitive both in terms of cost and weight. However, the main area of interest was the predicted effect of blade deflection on the hydrodynamic performance characteristics of the turbine and as such these limitations were deemed acceptable, at least at this stage of the study. The range of modulii used for the study was between 10 GPa and 200 GPa which are typical values of glass filled composites and steel, respectively.

3.4. Constraints and loads

Each of the 2,3 and 4 bladed rotor models were constrained by applying a remote displacement to the rear face of the hub as illustrated by the 2 bladed rotor in Fig. 3(A). The constraint was set with a displacement of 0 m in the x, y and z directions and a rotation of 0 rads about the x, y and z global axes. A rotational velocity matching that of the MRF in the CFD model was applied to the whole body of the turbine so that centrifugal force could be applied to the rotor structure, (B). The hydrodynamic loading and returned displacement on each blade is controlled via system coupling via fluid solid interfaces (C).

3.5. Analysis settings

The coupling sequence was set up such that the FEA model was solved first, followed by the CFD model. Table 1 gives an example mapping summary for the data transfers between the structural and fluid interfaces. It can be seen that a minimum of 93% mapping was achieved which, given the hardware constraints, was considered to be reasonable.

4. Discussion

As a first order approximation to the effects of blade deflection on kinetic energy extraction the 2-way FSI coupling procedure, as discussed, was used to predict shaft torque, axial thrust, maximum blade tip deflection and shaft power [19]. A baseline model was run with an upstream flow velocity of 3.086 m/s and rigid blades. The power was calculated by summing the local torques over the rotor blade surfaces and multiplying by the rotational velocity applied to the MRF. The power was then non-dimensionalised by dividing the extracted power by the total available power to give the power coefficient. Figures of power, torque and thrust coefficient against λ are given in Ref. [19]. Following the convergence of the power coefficient in the system coupling iterations for the flexible blade models, the baseline case of a rigid blade was used to normalise the power and thrust coefficients. Using 12 2.66 GHz processors, a runtime of approximately 340 h was required for each data point presented in the torque, power and deflection curves. Due to problems with inverted cells associated with dynamic meshing the lowest modulus reached in each of the models is not the same. These problems will be investigated in further studies however the following results do give a valuable insight to the effects of blade

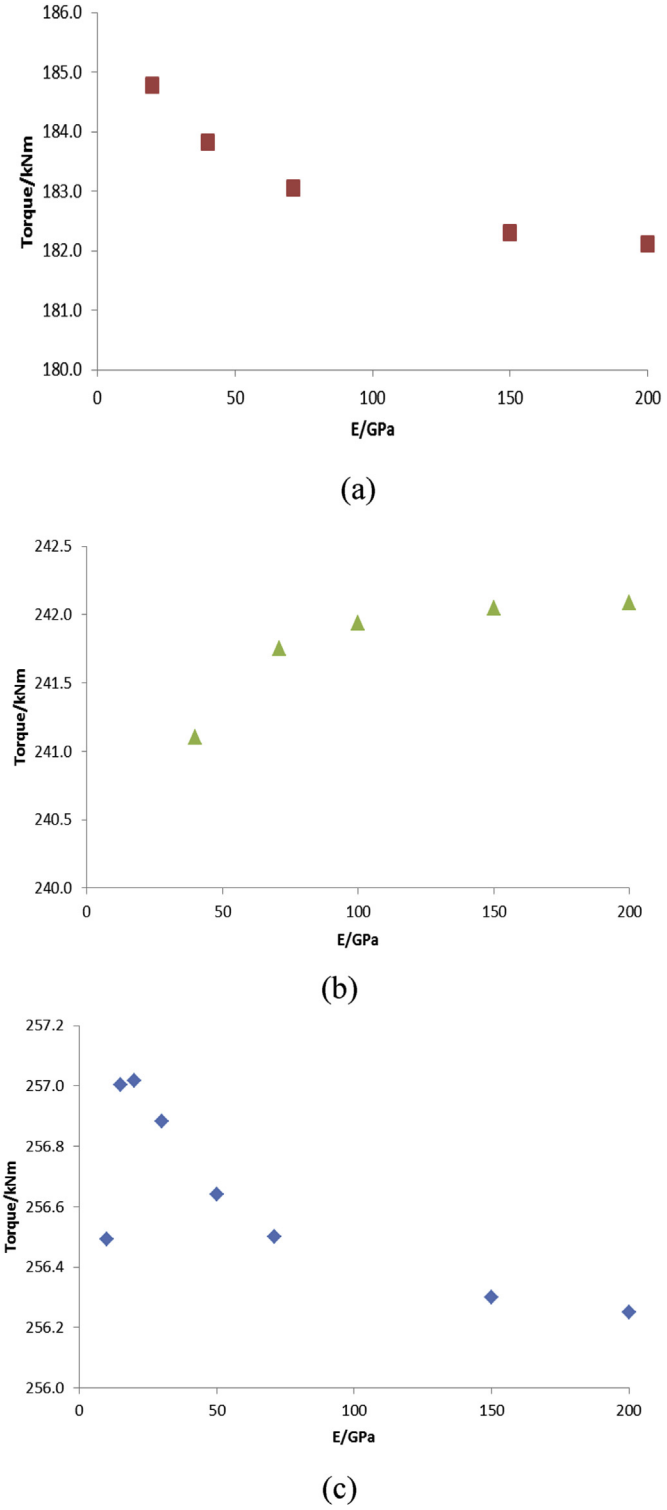

Fig. 4. Variation in shaft torque with reducing blade modulus { (a) 2-blade, (b) 3-blade, (c) 4-blade }.

deflection of kinetic energy extraction and thrust forces.

4.1. Variation in torque with reduction in blade material modulus for 2, 3 and 4 bladed rotors

It is evident from Fig. 4 that the resulting shaft torque is dependent on the number of turbine blades as each of the cases show a different performance with material modulus attenuation. As expected across the three cases there is a general increase of shaft torque with an increase in the number of blades. Although over a small range, it can be seen for the 2 blade rotor case (a) that the shaft torque increases as the modulus of the material is reduced: with a maximum shaft torque generated at a modulus of 20 GPa. This suggests that for the 2 blade rotor, the blade pitch angle is not fully optimised. Although not shown in Fig. 4 (a) it is reasonable to assume that the shaft torque will not continue to increase as the material modulus is further reduced below 20 GPa. Also that there must be a zero gradient and finally a reduction in the power output as the blade begins to deflect outside its operational range. The trend for the 3 bladed rotor (b) shows that the shaft torque increases with increasing material modulus. The shaft torque gradient starts to decrease at approximately 65 GPa and then tends toward zero as the material is further stiffened. The trend shown in Fig. 4 (b) suggests that the 3 blade rotor is optimised with maximum shaft torque being generated with minimum blade deflection. From this it would be sensible to adjust the blades with a predefined positive blade deflection, such that while operating, the blade deflects to its optimum hydrodynamic displacement. The 4 blade rotor has a similar trend to the 2 blade rotor, in that the generated shaft torque increases with a reduction in the material modulus, which produces a maximum torque of 257 kNm at a modulus of approximately 20 GPa. Following a peak of 257 kNm the shaft torque drops off to approximately 256.5 kNm: although the 0.5 kNm torque reduction is small, it indicates that a sudden small change in displacement has the potential to effect torque. As outlined in Ref. [18]: taken as a one-off, small changes in shaft torque (here less an 0.5%) could be considered as negligible, however over the life cycle of individual components small torque or power oscillations have the potential to induce structural failure and or long term efficiency losses. If it is presumed that the blade were to continue to deform, and given the rate of torque decay, the potential for fatigue loading also increases.

4.2. Variation in axial thrust with reduction in blade material modulus for 2, 3 and 4 blade rotors

From Fig. 5 it is apparent that the axial thrust data follows a similar trend to that of the shaft torque as the material stiffness is increased for the 2, 3 and 4 blade rotor configurations. The 2 blade data shows that the axial thrust force increases with shaft torque and decreasing blade stiffness. Below a modulus of 20 GPa it is hypothesised that the thrust force for the 2 bladed rotor (a) would continue to increase but at a lower rate, provided λ is maintained. For the 3 blade configuration (b) the axial thrust force increases as the material stiffness increases, however the

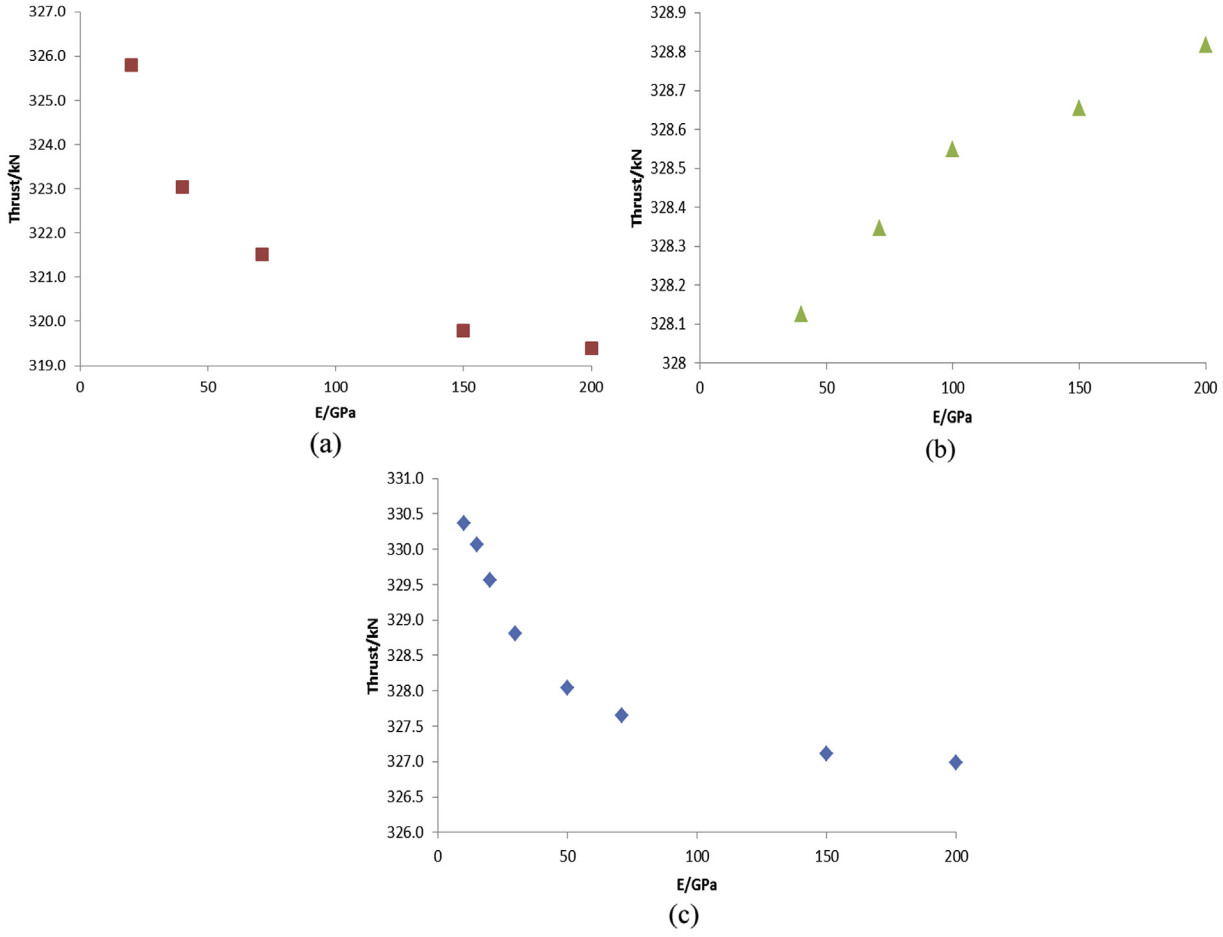

Fig. 5. Variation in total thrust force on turbine with material modulus { (a) 2-blade, (b) 3-blade, (c) 4-blade }.

rate of increase decreases as the material starts to tend towards a relatively rigid structure. Fig. 5 (c) shows that, as with the 2 blade turbine, the axial thrust load on the 4 blade turbine increases with decreasing modulus, although at the lowest value of modulus (10 GPa) the rate at which the thrust force increases starts to reduce.

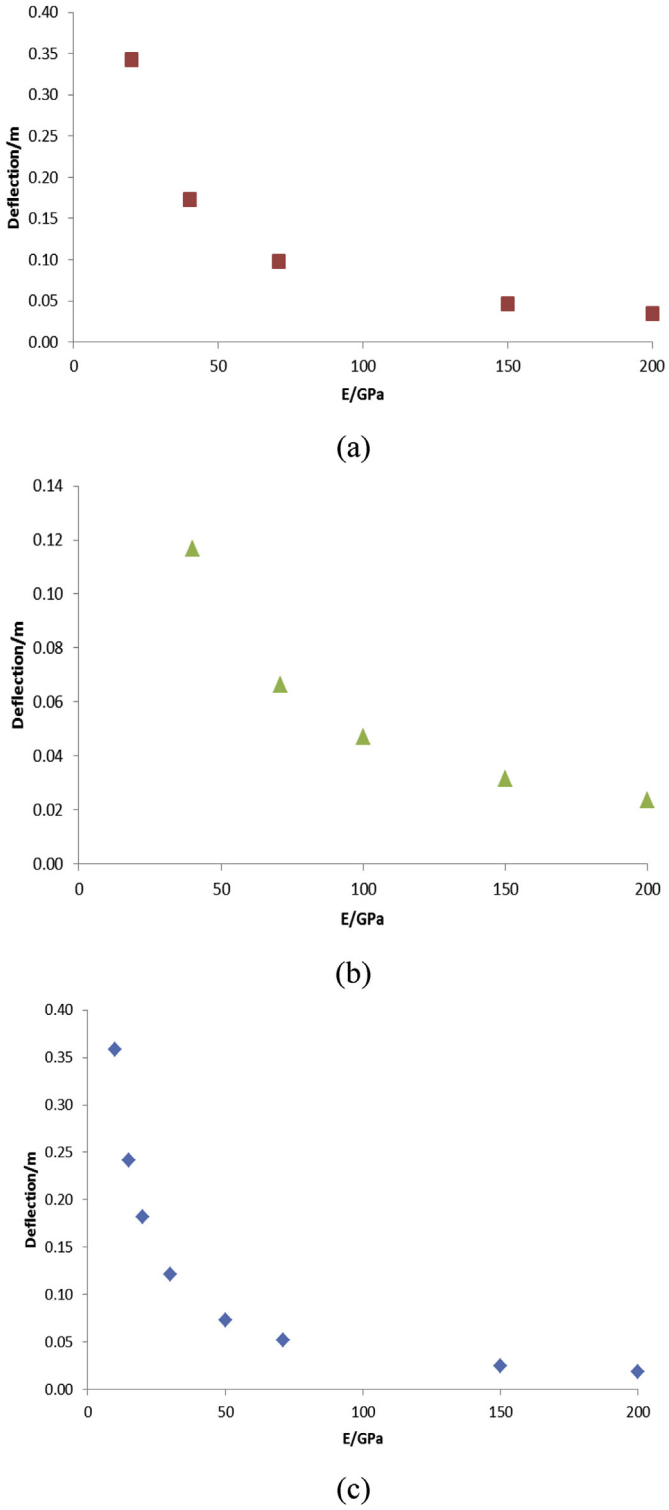

Fig. 6. Variation in blade tip deflection with material modulus { (a) 2-blade, (b) 3-blade, (c) 4-blade }.

4.3. Variation in maximum blade tip deflection with reduction in blade material modulus for 2, 3 and 4 blade rotors

Fig. 6 (a), (b) and (c) gives the maximum blade tip deflection for 2, 3 and 4 blade rotor configurations with decreasing material stiffness. As expected the deflection of the blades all follow a similar trend as the material stiffness is reduced. Clearly, as expected, the blade deflection increases with decreasing modulus. The deflection is shown to follow a power law, where the deflection changes by a factor which is the inverse of that by which the modulus is changed. For example, for the 2 blade rotor the deflection at 200 GPa is 0.035 m and this has increased to 0.35 m at a modulus of 20 GPa. It should be noted that the maximum deflection in each of the models was also limited by problems associated with dynamic remeshing during the FSI coupling. However the deflection results cover enough of their individual ranges to allow a reasonable estimation of the first order effects results from blade deflection. All the 2, 3 and 4 bladed rotor models cover the range between 200 GPa and 40 GPa and it is clear within this range that the 2 bladed rotor Fig. 6 (a) has the greatest degree of maximum blade tip deflection at 0.17 m. The maximum blade tip deflection for the 3 and 4 bladed rotors, Figures (b) and (c) are approximately 0.12 m and 0.11 m, respectively. For the 2 and 4 bladed rotors (a) and (c) it can be seen that the rate of maximum blade tip deflection starts to increase below a modulus of 40 GPa and it is expected that the 3 bladed rotor (b) will follow a similar trend to that of the 2 and 4 bladed rotors. Although not covered in detail for this paper is was shown by Morris [19] that the total axial thrust load is of the same order of magnitude for each rotor configuration the thrust per blade will be highest for the 2 blade and lowest for the 4 blade rotors. This explains why deflection increases with decreasing number of blades as shown in the trends of displacement vs modulus E, Fig. 7. Again it is important to note that these changes in displacement have more of an impact on cyclic loading and fatigue than a steady state displacement, as discussed in this paper.

4.4. Variation in power extraction with reduction in blade material modulus for 2, 3 and 4 blade rotors

Fig. 8 (a), (b) and (c) gives the amount of shaft power generated

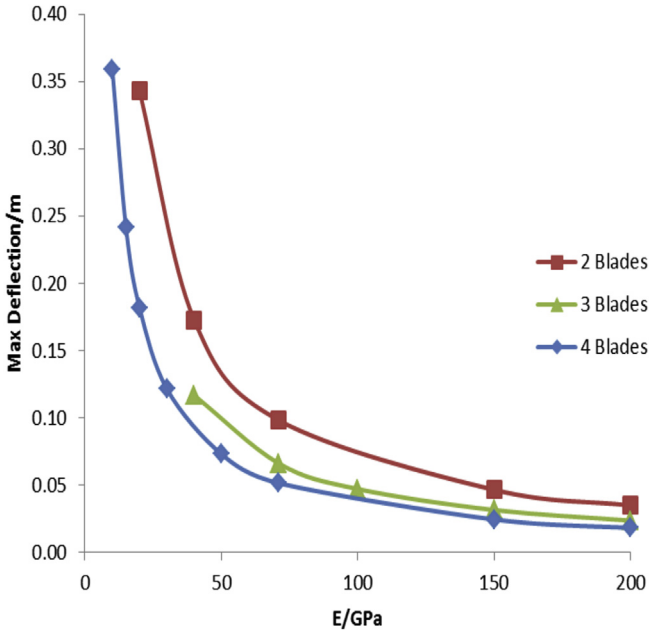

Fig. 7. Deflection vs E for the 2, 3 and 4 bladed turbines.

against the maximum blade tip deflection as a result of reducing blade stiffness. As indicated by the torque data (Fig. 4) for the 2 blade rotor Fig. 8 (a) shows that the power generated increases by 7.3 kW with deflection of 0.35 m indicating that the blade geometry is not currently optimised for the 2 bladed rotor in its rigid state. With the exception of a 500 W increase at 0.022 m the general trend for the 3 blade rotor (b) is that the generated power decreases as the maximum blade tip deflection increases. A decrease of around 2.5 kW is indicated with a deflection of 0.118 m and therefore demonstrating that the current 3 blade rotor is slightly sensitive to blade deflections above 0.03 m. In its 3 blade configuration the rotor is likely to be too rigid and would therefore benefit from a structure that allows for higher blade deflection. Fig. 8 (c) shows that the shaft power of the 4 bladed rotor increases to a maximum of approximately 539.7 kW from a base state of around 537.8 kW at deflections of 0.000 m and 0.182 m, respectively. The approximate 2 kW increase in the power extracted is then followed by a 1 kW decrease in the power extracted as the blade tip deflection increases to 0.359 m. It is likely that a similar trend would be apparent in the 2 blade rotor as for the 4 blade rotor, in that the shaft power would start to decrease after a deflection of approximately 0.37 m. It is clearfrom Fig. 8 (c) that the optimum power extraction for the 4 blade rotor does not occur at 0 m deflection, since a peak occurs at 0.2 m deflection. However, this is not necessarily the optimum position for this blade as other deformations with different combinations of bending and twisting have the potential to further increase the extracted power.

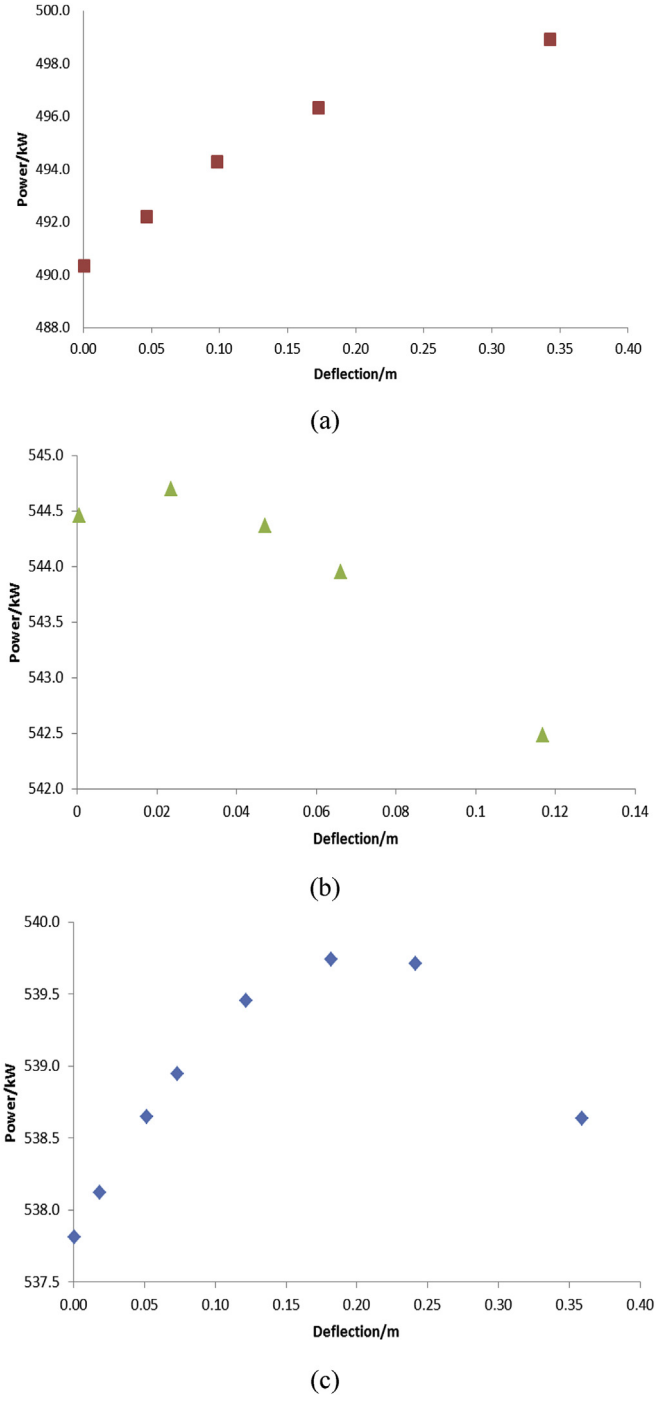

Fig. 8. Variation in shaft power with maximum blade tip deflection { (a) 2-blade, (b) 3-blade, (c) 4-blade }.

To allow for a comparison between the three rotor configurations Fig. 9 shows the power output against deflection normalised against a rigid blade and therefore zero deflection. When compared to the rigid structure it is clear from Fig. 9 that the 2 blade rotor shows an increase in power extraction as the blades deflect away from their rigid state. The deflection also changes the pitch angle and so the apparent angle of attack. It should be noted that over the deflection range studied, the 2 blade rotor has not reached peak power extraction. To a lesser extent this is also shown for the 4 blade rotor, although here a peak power extraction occurs around a deflection of 0.2 m which then decreases toward the rigid blade normalised result as the deflection approaches 0.4 m. Fig. 9 also suggests that the 3 blade rotor is close to the optimum pitch angle before deformation.

As the blades deflect as a result of the thrust loading, the tip pitch angle increases. Fig. 10 shows how the power changes with the increase in pitch angle for the 2, 3 and 4 bladed turbines. The trends are similar to the curves of power against deflection and suggest that the 3 bladed turbine is close to optimum pitch angle in its original undeflected state, whereas the 4 bladed turbine is around 0.3° out and the 2 bladed turbine is at least 0.4° out. This could explain why the power output of the 2 and 4 bladed turbines increases with blade deflection despite the small reduction in swept area. Along with the change in tip pitch angle, there is also a

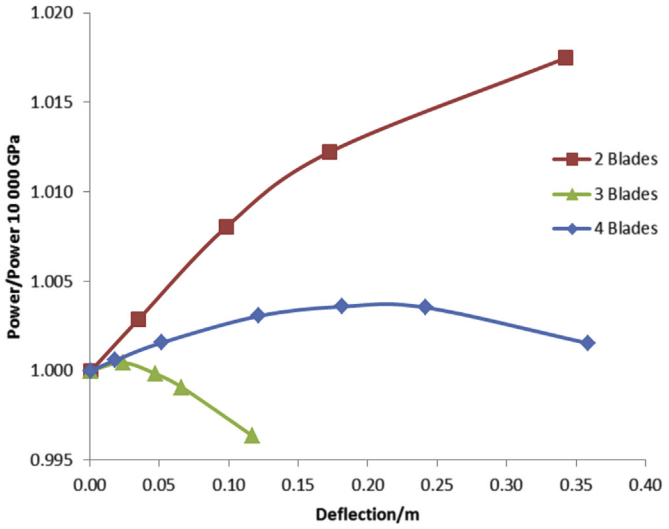

Fig. 9. Normalised power vs deflection for the 2, 3 and 4 blade turbines.

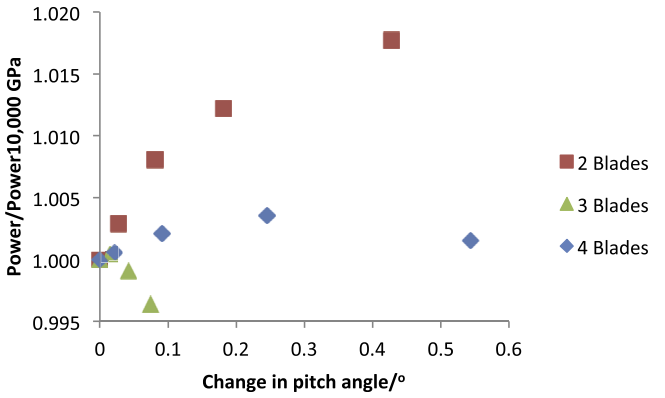

Fig. 10. Normalised power vs change in pitch angle for the 2, 3 and 4 bladed turbines.

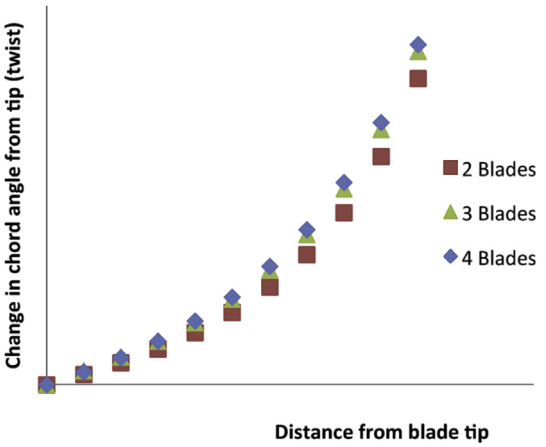

Fig. 12. Twist required to maintain a constant angle of attack at λ for peak power found in this study.

change in the twist along the length of the blade, reducing the difference between the angle at the tip of the blade and the base of the blade. Fig. 11 shows how the power changes as the twist from base to tip reduces. It is not possible to separate the effect of the change in pitch angle from the change in twist or to determine how much influence each of these variables has on the power. However, since the power output of the 3 bladed turbine increases slightly and then decreases with changes of pitch angle and of twist, it is likely the original position is close to optimum for both variables.

Fig. 12 shows the variation in angle along a blade that would be required to maintain a constant angle of attack based on the values of λ associated with peak C_p for each turbine, relative to each other. It is clear that the required twist increases with the number of blades. Although the effect of the reduction in twist with deflection, seen in Fig. 11, may be small, when combined with the increase in tip pitch angle, could explain the 1.7% increase in power seen for the 2 bladed turbine. Since the required twist is slightly higher for the 4 bladed turbine than for the 3 bladed turbine, the reduction in twist with deflection would be expected to result in a reduction in power. This could explain why the change in power output of the 4 bladed turbine is smaller than that of the 2 bladed turbine as the tip pitch angle moves closer to optimum but the twist moves further from optimum. The reduction in power seen for the 3 bladed turbine could be a result of both tip pitch angle and twist moving away from the optimum position as the blade deflects.

To increase confidence that changes in power observed with blade deflection were not due to numerical error, the 2 blade turbine model was run as a rigid CFD model with small variations in tip pitch angle. The results were then compared with those from the 2-Way Coupled FSI model, as shown in Fig. 13. The 2 blade rotor was chosen because of its lower mesh density and hence lower computational expense. From Fig. 13 it is clear that, although there is a difference between the data sets, they show good general agreement.

5. Conclusions

Blade deformation and associated changes in performance characteristics were investigated using static 2-way Fluid Structure Interaction (FSI). The aim of the investigation was to better understand the effect of blade deformation on kinetic energy extraction by varying the material modulus and hence the stiffness of the rotor structure. Shaft torque/power, maximum blade tip displacement, and axial thrust results were presented for 2, 3 and 4 blade rotor configurations. Blade deflection was shown to increase with a reduction in the number of blades, due the increased thrust per blade. The power output of the 3 blade turbine was shown to decrease with deflection, whereas for the 2 and 4 bladed turbines it was found to first increase as it was subsequently found that the pitch settings were not fully optimised. The power output of the 4 bladed turbine was found to initially increase with deflection and then decrease with further deflection. It is expected that the power output of the 2 blade turbine would eventually decrease with further deflection but no decrease was found for the maximum deflection obtain in this work. It was therefore found that blade deflection will alter the power output and that blades could be designed so as to reach their optimum setting at a given blade

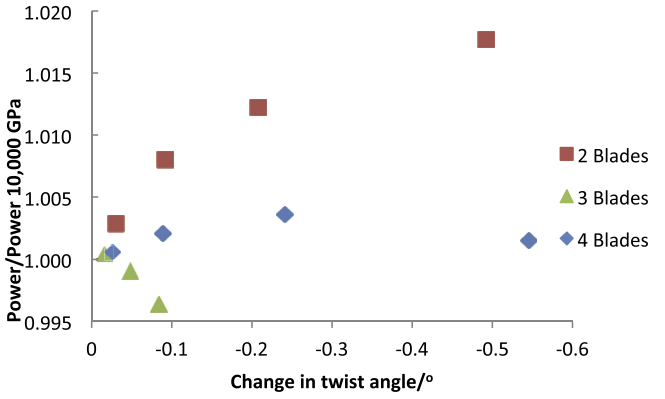

Fig. 11. Normalised power vs change in twist angle for the 2, 3 and 4 bladed turbines.

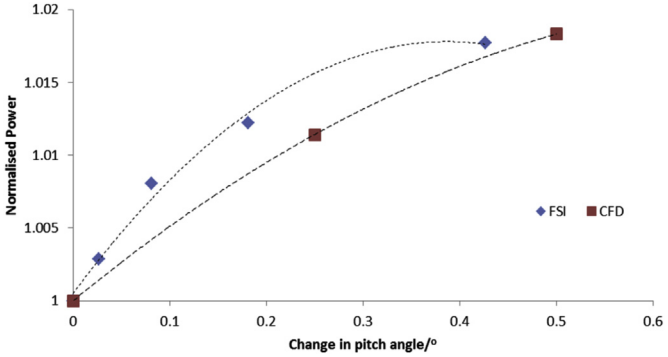

Fig. 13. Normalised power for 2 bladed rotor vs change in pitch angle (normalised against E = 10,000 GPa).

deflection. Overall, and in agreement with [18] the FSI model data demonstrated that the performance sensitivity to blade deformation for the 2, 3 and 4 bladed rotor is low, but should not be neglected. It was also shown that the magnitude of the deflection and hence performance could be significantly influenced by the relationship between the optimised pitch angle via a rigid and deformable model. Future studies will include stanchion rotor interaction and the effects of smaller perturbations when considering fatigue.

Acknowledgements

The authors gratefully acknowledge the financial support from EPSRC (EP/j010200/1) and LCRI (Ref: 80366) for funding C. Morris and A. Mason-Jones.

References

[1] European Union Committee, 27th Report of Session 2007–08-The EU's Target for Renewable Energy: 20% by 2020, The Stationery Office Limited, London, 2008.
[2] DECC, UK Renewable Energy Roadmap, Crown Copyright, Department of Energy & Climate Change, London, 2011.
[3] DECC, UK Renewable Energy Roadmap Update 2012, Crown Copyright, Department of Energy & Climate Change, London, 2012.
[4] Carbon Trust, Accelerating Marine Energy: the Potential for Cost Reduction: Insights from the Carbon Trust Marine Energy Accelerator, 2011.
[5] V. De Laleu, La Rance Tidal Power Plant. 40-year Operation Feedback – Lessons Learnt BHA Annual Conference, 2009. www.british-hydro.org/downloads/La%20Rance-BHA-Oct%202009.pdf (accessed July 2014).
[6] Tidal Lagoon, E-Newsletter No 10, 2014 [Online]. Available at: http://www.tidallagoonswanseabay.com/document-library.aspx (accessed 20.03.13).
[7] Carbon Trust, Accelerating Marine Energy: the Potential for Cost Reduction: Insights from the Carbon Trust Marine Energy Accelerator, 2011.
[8] Royal Haskoning, SeaGen Environmental Monitoring Programme Final Report, 2011 [Online]. Available at: http://www.marineturbines.com/sites/default/files/SeaGen-Environmental-Monitoring-Programme-Final-Report.pdf (accessed 02.03.13).
[9] C.B. Byrne, R.I. Grosvenor, A. Mason-Jones, C.E. Morris, D.M. O'Doherty, T. O'Doherty, P.W. Prickett, Consideration of the condition based maintenance of marine tidal turbines, in: 9th European Wave and Tidal Energy Conference (EWTEC), 2011.
[10] L. Yin, Michael R. Motley, Ronald W. Yeung, Three-dimensional numerical modelling of the transient fluid-structural interaction response of tidal turbines, J. Offshore Mech. Artic Eng. 132 (February 2010).
[11] G. Ingram, Wind Turbine Blade Design Analysis Using he Blade Element Momentum Method, Version 1.1, School of Engineering, Durham University, 2011. http://community.dur.ac.uk/g.l.ingram/download/wind_turbine_design.pdf (accessed 26.06.14).
[12] A. Bahaj, W. Batten, G. McCann, Experimental investigations of numerical predictions for the hydrodynamic performance of horizontal axis marine current turbines, Renew. Energy 32 (2007) 2479–2490.
[13] W. Batten, A. Bahaj, A. Molland, J. Chaplin, S.E.R. Group, Experimentally validated numerical method for the hydrodynamic design of horizontal axis tidal turbines, Ocean. Eng. 34 (2007) 1013–1020.
[14] N. Barltrop, K. Varyani, A. Grant, D. Clelland, X. Pham, Investigation into wave-current interactions in marine current turbines, Proc. Mech. Part J. Power Energy 221 (2007) 233–242.
[15] R. Malki, A.J. Williams, T.N. Croft, M. Togneri, I. Masters, A coupled blade element momentum – Computational fluid dynamics model for evaluating tidal stream turbine performance, Appl. Math. Model. 37 (2013) 3006–3020.
[16] W.M.J. Batten, M.E. Harrison, A.S. Bahaj, Accuracy of the actuator disc-RANS approach for predicting the performance and wake of tidal turbines, Philos. Trans. R. Soc. A Math. Phys. Eng. Sci. 371 (2013) 20120293.
[17] R.F. Nicholls-Lee, S.R. Turnock, S.W. Boyd, A method for analysing FSI on a HATT, in: 9th European Wave and Tidal Energy Conference, September 2011, pp. 5–9. Southampton.
[18] S.W. Park, S. Park, S.H. Rhee, Performance predictions of a horizontal axis tidal stream turbine considering the effects of blade deformation, in: 3rd International Symposium on Marine Propulsors, May 2013, pp. 5–8. Launceston.
[19] C. Morris, Influence of Solidity on the Performance, Swirl Characteristics, Wake Recovery Blade Deflection of a Horizontal Axis Tidal Turbine, Cardiff University, 2014. PhD thesis.
[20] C. Morris, A. Mason-Jones, D.M. O'Doherty, T. O'Doherty, Evaluation of the swirl characteristics of a tidal stream turbine wake, Int. J. Mar. Energy (2015). No:IJOME-D-14–00034R1, (Available online 29 August 2015), http://dx.doi.org/10.1016/j.ijome.2015.08.001.
[21] A. Mason-Jones, Performance Assessment of a Horizontal Axis Tidal Turbine in a High Velocity Shear Environment, Cardiff University, 2010. PhD thesis.
[22] D.M. O'Doherty, A. Mason-Jones, T. O'Doherty, C.B. Byrne, I. Owen, Y.X. Wang, Experimental and computational analysis of a model horizontal axis tidal turbine, in: 8th European Wave and Tidal Energy (EWTEC 2009), 2009.
[23] A. Mason-Jones, D.M. O'Doherty, C.E. Morris, T. O'Doherty, C.B. Byrne, P.W. Prickett, R.I. Grosvenor, I. Owen, S. Tedds, R.J. Poole, Non-dimensional scaling of tidal stream turbines, Energy 44 (1) (2012) 820–829, 0360-5442 10.1016/j.energy.2012.05.010.
[24] ANSYS, Fluent Documentation, 2014.